Spiral Spectrum of a Laguerre-Gaussian Beam Propagating in Anisotropic Turbulent Plasma

Yankun Wang, Lu Bai, Danmeng Zhang, Jinyu Xie, Ya Guo, and Lixin Guo

***Abstract*—The explicit expression of orbital angular momentum (OAM) spiral spectrum of Laguerre-Gaussian (LG) beam propagating in anisotropic plasma turbulence is derived based on Rytov theory. The relationship between the detection probability of OAM and the crosstalk with the anisotropy parameters, topological charge, radial index, wavelength, beam width, receiving aperture, inner and outer scales are discussed in detail. In order to quantify the effect of plasma turbulence, we compared it with atmospheric turbulence based on restriction function. To optimize OAM detection probability, we also compared the effects of circular aperture method (CAM) with focusing mirror method (FMM) on the propagation characteristics of the spiral spectrum. The results show that even in the strong turbulence region of atmospheric turbulence, the radial dimension of LG beam in plasma turbulence is nearly twice that of atmospheric turbulence and the modes crosstalk has almost reached its upper bound. Besides, by comparing the two optimization methods, we found the ability to reduce crosstalk is related to the choice of beam width and receiving aperture. Therefore, we give a method to optimally select between the CAM and the FMM. We found the corresponding relationship and gave an analytical formula. The FMM has a greater ability to reduce crosstalk than the CAM when the beam width $\geq$4 cm and the aperture $\geq$3 cm. We quantified the effect of plasma turbulence and provide a guideline for the selection of beam width and receiving aperture under these two optimization methods. The research results may be helpful in the field of optical communication.**

***Index Terms*—Orbital angular momentum, spiral spectrum, anisotropic turbulence.**

I. Introduction

WHEN an aircraft is flying at hypersonic speeds in the atmosphere, the aircraft rub with the surrounding air causes the gas molecules to ionize and form anisotropic plasma turbulence (also known as plasma sheath), which can perturb communication with the aircraft [1]. In severe cases, the communication link will be interrupted, resulting in "blackout" [2], [3].

Manuscript received August 31, 2021; revised October 6, 2021; accepted October 7, 2021. Date of publication October 12, 2021; date of current version November 4, 2021. This work was supported by the National Natural Science Foundation of China under Grants 61875156 and U20B2059. *(Corresponding author: Lu Bai.)*

Yankun Wang, Danmeng Zhang, Jinyu Xie, and Ya Guo are with the School of Physics and Optoelectronic Engineering, Xidian University, Xi'an 710071, China (e-mail: wangyk@stu.xidian.edu.cn; dmzhang1@stu.xidian.edu.cn; jinyu_xie@stu.xidian.edu.cn; yaguo@stu.xidian.edu.cn).

Lu Bai is with the School of Physics and Optoelectronic Engineering and Collaborative Innovation Center of Information Sensing and Understanding, Xidian University, Xi'an 710071, China (e-mail: blu@xidian.edu.cn).

Lixin Guo is with the School of Physics and Optoelectronic Engineering, Xidian University, Xi'an 710071, China (e-mail: lxguo@xidian.edu.cn).

Digital Object Identifier 10.1109/JPHOT.2021.3119337

Theories and experiments show that terahertz waves [4]–[7] or high-frequency light waves [8]–[10] can pass through plasma sheath relatively low-frequency electromagnetic waves, and the signal loss is very small, which provides a new idea to alleviate the "blackout" problem. In the early research, many researchers used ray tracing and geometric optics methods, mainly focusing on physical quantities such as optical path differences (OPD) [11]–[13] and Strehl ratios (SR) [14], [15]. Some researchers also regard the shock layer as a strongly turbulent medium and use the refractive index power spectrum of atmospheric turbulence to layer the sheath to study the propagation and distortion characteristics of optical beam and the influence on imaging quality [16], [17]. The turbulence intensity can reach 10^{-12}. Instead, in the field of computational electromagnetics, more attention is paid to the electron density [18]–[20] or collision frequency [21], [22] of this medium. Theories and experiments also show that the hypersonic plasma sheath has turbulent characteristics [23], [24]. Therefore, similar to the atmospheric turbulence, it also follows the statistical average theory. The effect of isotropic plasma turbulence on the beam has been fully studied. Li *et al.* studied the propagation characteristics of Gaussian beams in plasma turbulence, focusing on the average irradiance, scintillation index, fluctuations of the arrival angle and beam spreading of the Gaussian beams [25]. In 2017, Yang *et al.* studied the bit error rate (BER) performance of free-space optical links under the influence of plasma turbulence [26]. Lyu *et al.* studied the propagation characteristics of Gaussian beams in plasma turbulence based on the random phase screen method in 2019 [27]. Due to the anisotropy exhibited by the large-scale structure of turbulent vortices, on the basis of processing the experimental images of hypersonic turbulence [28], Li *et al.* transformed the anisotropic von Kármán spectrum to obtain the anisotropic power spectrum of the refractive index fluctuations of the hypersonic turbulence in 2016 [29]. The wave structure function and spatial coherence radius of wave propagating in hypersonic turbulence are derived. This has greatly promoted the study of the propagation characteristics of optical waves in hypersonic plasma turbulence. Huang *et al.* studied the statistical properties of Gaussian Schell-model beams in anisotropic hypersonic turbulence [30]. However, the influence of the anisotropy of plasma turbulence on the OAM is rarely reported. In order to promote the communication of hypersonic vehicles, it is necessary to study the effect of this anisotropic plasma turbulence on the beam.

Allen *et al.* had proved in 1992 that new kind of optical field with phase factor $\exp(i\ell\varphi)$ can carry OAM, where ℓ is

an arbitrary integer, represents the topological charge, and φ is azimuth coordinate [31]. Owing to the orthogonality and completeness of OAM, it has been proved that OAM has infinite dimensional Hilbert space and can carry infinite dimensional information. In principle, it is allowed to increase the channel transmission capacity. Thus, it has been widely used in the field of high-performance optical communications in free space and turbulent environments [32]–[38]. Gbur *et al.* simulated and analyzed the propagation of vortex beams in weak-to-strong atmospheric turbulence in 2008 [39]. The results show that the topological charge of the vortex beam is a robust quantity that could be used as an information carrier for optical communication. The spiral spectrum propagation and crosstalk characteristics of OAM directly reflect the communication performance of the corresponding channel, it has far-reaching research significance. In recent years, many references have reported the propagation characteristics of the spiral spectrum of vortex beams in atmospheric turbulence, including LG beams [40], Bessel-Gaussian beams [41], Lommel-Gaussian beams [42] and so on [43]. In terms of anisotropic plasma turbulence, Li *et al.* reported the polarization characteristics of radially polarized partially coherent vortex beams in anisotropic plasma turbulence in 2020, mainly focusing on intensity distribution evolution and generalized polarization degree [44]. Xu *et al.* studied the OAM propagation characteristics and time evolution of LG beam in the supersonic turbulence boundary layer [45]. However, there are few reports on the propagation characteristics of the vortex beam spiral spectrum in hypersonic plasma turbulence. Among many OAM beams, LG beams are considered by many researchers as the best candidates for free-space optical communication links due to their natural generation and stable propagation. Therefore, this paper focusing on the spiral spectrum characteristics of the LG beam propagating in the plasma turbulence.

In this paper, we investigated the specific of anisotropic plasma turbulence on the transmission characteristics of the LG beam OAM spiral spectrum. The influence of plasma turbulence on OAM is quantified and an optimization scheme is proposed. The research results are useful for parameter optimization and selection based on OAM transmission in plasma turbulence and can be generalized.

This paper is organized as follows: In Section II, the refractive index fluctuation power spectrum model of anisotropic plasma turbulence is reviewed; In Section III, based on the Rytov approximation, the theoretical model for calculating the OAM spiral spectrum of the LG beam propagating in plasma turbulence is derived; In Section IV, by numerical simulation, the effects of the turbulence parameters (that is, anisotropic parameters, outer scales and refractive index fluctuation variance) and beam parameters (topological charge, radial index, wavelength, beam width and receiving aperture) on the propagation of the LG beam OAM spiral spectrum are discussed; In Section V, we quantified the effect of plasma turbulence based on the restriction theory and compared with the atmospheric turbulence. In Section VI, we compare and analyze the circular aperture and focusing mirror optimization methods of spiral spectrum and provide a guideline for the selection of beam width and receiving aperture; Section VII presents the conclusion.

II. Anisotropic Power Spectrum for Plasma Turbulence

The anisotropic refractive index power spectrum of plasma turbulence is transformed from the modified von Kármán spectrum, expressed as follows [29]

$$\Phi(\kappa) = a_1 \frac{64\pi \left\langle n_1^2 \right\rangle L_0^2 \left(m_1 - 1\right)}{\left(1 + 100\kappa L_0^2\right)^{m_1}} \exp\left(-\frac{\kappa}{\kappa_0}\right). \quad (1)$$

where $\kappa \equiv (\kappa_x, \kappa_y)$ is the transverse spatial frequency, $\langle n_1^2 \rangle$ is the variance of the refractive-index fluctuation; l_0 and L_0 are the inner and outer scales, respectively; $\kappa_0 = (2\pi/l_0)^{m_1 - 0.7}$, where $m_1 = 4\text{-}d$, in which d is the fractal dimension; the parameter a_1 is a fitting parameter, which can be expressed as a function of κ_0 and m_1. For the fully developed turbulence in turbulence mixing layer, $d = 2.6$, and thus $m_1 = 1.4$.

Note that the relationship between L_0 and l_0 satisfies [46]

$$\frac{L_0}{l_0} = {R_e}^{3/4}. \quad (2)$$

where the Reynolds number $R_e = 5 \times 10^5$.

The plasma turbulence is a turbulent shear flow. Refer to the Nano-based Planar Laser Scattering (NPLS) experiment image [13]. The plasma turbulence has the characteristics of non-uniform and anisotropic. Considering the large-scale asymmetric structure of turbulence eddies on the path, the anisotropic spectrum is given by [29], [47]

$$\Phi\left(\kappa'\right) = a_1 \frac{64\pi \left\langle n_1^2 \right\rangle L_0^2 \left(m_1 - 1\right)}{\left(1 + 100\kappa' L_0^2\right)^{m_1}} \exp\left(-\frac{\kappa'}{\kappa_0}\right). \quad (3)$$

where $\kappa\prime = \sqrt{\xi_x^2\kappa_x^2 + \xi_y^2\kappa_y^2 + \kappa_z^2}$; ξ_x and ξ_y are two anisotropy parameters representing scale-dependent stretching along the x and y directions, respectively. If $\xi_x = \xi_y = 1$, (3) reduce to the isotropic power spectrum (1).

III. Theoretical Model of the OAM Mode for a LG Beam Propagating in Anisotropic Plasma Turbulence

We now consider how to use the model in the previous section to simulate the propagation of LG beam in anisotropic plasma turbulence. Due to the existence of turbulence, even if the OAM mode of the input plane is pure, the OAM mode spectrum of the receiving plane will be spread. In this case, the optical field of the LG beam at the receiver plane in the absence of turbulence can be given as [48]

$$LG_p^{(\ell)}\left(r, \varphi, z\right) = S \times \exp\left(i\ell\varphi\right), \quad (4)$$

where

$$\begin{aligned} S = {} & \sqrt{\frac{2p!}{\pi\left(p + |\ell|\right)!}} \frac{1}{w\left(z\right)} \left[\frac{r\sqrt{2}}{w\left(z\right)}\right]^{|\ell|} L_p^{(|\ell|)}\left[\frac{2r^2}{w^2\left(z\right)}\right] \\ & \times \exp\left[-\frac{r^2}{w^2\left(z\right)}\right] \exp\left[\frac{ikr^2 z}{2\left(z^2 + z_R^2\right)}\right] \\ & \times \exp\left[-i\left(2p + |\ell| + 1\right)\tan^{-1}\left(\frac{z}{z_R}\right)\right] \exp\left(i\ell\varphi\right) \quad (5) \end{aligned}$$

In Eq. (4) and (5), z refers the distance between the input plane and the receiver plane, r is the radial coordinates in a polar coordinate system. $w(z)$ is the fundamental Gaussian beam radius at the receiver plane and $w(z) = w_0\sqrt{1+(z/z_R)^2}$, w_0 is initial beam width, the Rayleigh range $z_R = \pi w_0^2/\lambda$, and $k = 2\pi/\lambda$ is the wave number, λ is the wavelength. $L_p^{(\ell)}(\cdot)$ is the associated Laguerre polynomial.

In the presence of turbulence, the optical field of the LG beam at the receiver plane under the Rytov approximation as [49]–[51]

$$U_{tur}(r,\varphi,z) = LG_p^{(\ell)}(r,\varphi,z)\exp[\psi(r,\varphi,z)], \quad (6)$$

where ψ (r, φ, z) is the complex random phase perturbation induced by the plasma turbulence.

According to [49], [52], to elucidate the OAM content, or spiral spectrum, of a field distribution U_{tur} (r, φ, z) one has to compute its projection into the spiral harmonics $\exp(im\varphi)$. Thus, we can write the function U_{tur} (r, φ, z) as a superposition of this spiral harmonics

$$U_{tur}(r,\varphi,z) = \frac{1}{\sqrt{2\pi}}\sum_{m=-\infty}^{\infty}\beta_m(r,z)\exp(im\varphi), \quad (7)$$

where m is an integer number, represents mutually orthogonal OAM modes, and the functions β_m (r, z) are given as

$$\beta_m(r,z) = \frac{1}{\sqrt{2\pi}}\int_0^{2\pi}U_{tur}(r,\varphi,z)\exp(-im\varphi)\,d\varphi, \quad (8)$$

The square of the modulus of β_m (r, z) is

$$\left\langle|\beta_m(r,z)|^2\right\rangle = \frac{1}{2\pi}\int_0^{2\pi}\int_0^{2\pi}U_{tur}(r,\varphi_1,z)\exp(-im\varphi_1) \times U_{tur}^*(r,\varphi_2,z)\exp(im\varphi_2)\,d\varphi_1 d\varphi_2, \quad (9)$$

where $\langle\cdots\rangle$ stands for the ensemble average, and $*$ denotes the complex conjugate. Substituting (6) into (9) and taking the ensemble average of the turbulent phase perturbations, we can obtain

$$\left\langle|\beta_m(r,z)|^2\right\rangle = \frac{1}{2\pi}\int_0^{2\pi}\int_0^{2\pi}LG_p^{(\ell)}(r,\varphi_1,z)\,LG_p^{(\ell)*}(r,\varphi_2,z) \times\exp[-im(\varphi_1-\varphi_2)]\langle\exp[\psi(r,\varphi_1,z) + \psi^*(r,\varphi_2,z)]\rangle d\varphi_1 d\varphi_2, \quad (10)$$

The $\langle|\beta_m(r,z)|^2\rangle$ represents the probability density of spiral modes in turbulence.

According to [53], the second-order statistics of the complex phase disturbance can be expressed as

$$\langle\exp[\psi(r,\varphi_1,z)+\psi^*(r,\varphi_2,z)]\rangle = \exp\left[-2r^2T(z)+2r^2T(z)\cos(\varphi_1-\varphi_2)\right], \quad (11)$$

where

$$T(z) = \frac{\pi^2k^2z}{3}\int_0^{\infty}\kappa^3\Phi_n(\kappa)\,d\kappa, \quad (12)$$

where $\Phi_n(\kappa)$ is the spectral power spectrum of the refractive index fluctuations shown in (3). Substituting (3) into (12) and applying the Markov approximation, (12) can be written as [54]

$$\begin{aligned}T(z) &= \frac{\pi^2k^2z}{3}\int_0^{\infty}\kappa^3\Phi_n(\kappa)\,d\kappa \\ &= \frac{32\pi^3k^2za\left\langle n_1^2\right\rangle {L_0}^2(m_1-1)}{3}\frac{{\xi_x}^2+{\xi_y}^2}{{\xi_x}^3{\xi_y}^3} \\ &\quad\times\left(\frac{1}{100{L_0}^2}\right)^4 U\left(4;5-m_1;\frac{1}{100{L_0}^2\kappa_0}\right)\times\Gamma(4),\end{aligned} \quad (13)$$

where $U(a;c;z)$ is the confluent hypergeometric function of the second kind.

Substituting (13) into (10), we obtain the final expression of the mode probability density for spiral modes

$$\left\langle|\beta_m(r,z)|^2\right\rangle = 2\pi SS^*\exp\left(-2r^2T\right)I_{m-\ell}\left(2r^2T\right), \quad (14)$$

where I_n is the modified Bessel function of the first kind with order n.

The total energy received by the detector can be written as [40], [55], [56]

$$E = 2\varepsilon_0\sum_{m=-\infty}^{\infty}C_m, \quad (15)$$

where

$$C_m = \int_0^R\left\langle|\beta_m(r,z)|^2\right\rangle r dr. \quad (16)$$

represents the energy content of each OAM mode, and R denotes the receiving aperture radius.

The energy fraction possessed by the m-th spiral harmonic of the LG beam after turbulent transmission is determined by the following expression

$$P_m = \frac{C_m}{\sum_{q=-\infty}^{\infty}C_q}. \quad (17)$$

Due to the disturbance effect of the plasma turbulence on the beam, the input OAM mode ℓ will degenerate during propagation, hence the value of P_m will decrease when $m = \ell$. In this case, $P_{m=\ell}$ can be regarded as the detection probability of signal OAM mode ℓ, which shows the transmission efficiency of the transmitted OAM mode. For $m = \ell+\Delta\ell$, define P_m as the crosstalk probability, which denotes the probability of a photon changing its OAM mode, and $\Delta\ell$ is the difference between the transmitted and received OAM mode.

IV. Numerical Results

This section presents the OAM spiral spectrum propagation characteristics of a LG beam in anisotropic plasma turbulence. Fig. 1 illustrates the detection probability of OAM modes under different anisotropy parameter ratios. The calculation parameters are: $\ell = 1$, $p = 0$, $\lambda = 1550$ nm, $w_0 = 2$ cm, $L_0 = 0.1$ m, $l_0 = 5\times10^{\supset 6}$ m, $\langle n_1^2\rangle = 0.73\times10^{-20}$, $R = 3$ cm. Since the experiment indicates that maximum of thickness of the anisotropic plasma flow field is 0.4 m, the propagation length is set as $z = 0.4$ m. It can be observed that the mode crosstalk mainly depends on the ratio of ξ_x/ξ_y. From Figs. 1(a)–(c), if we fixed ξ_x,

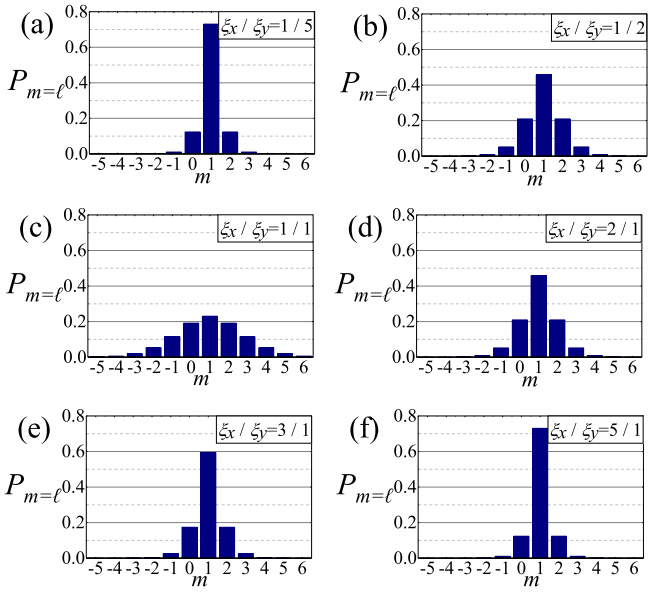

Fig. 1. Detection probability of OAM modes under different anisotropy parameter ratios.

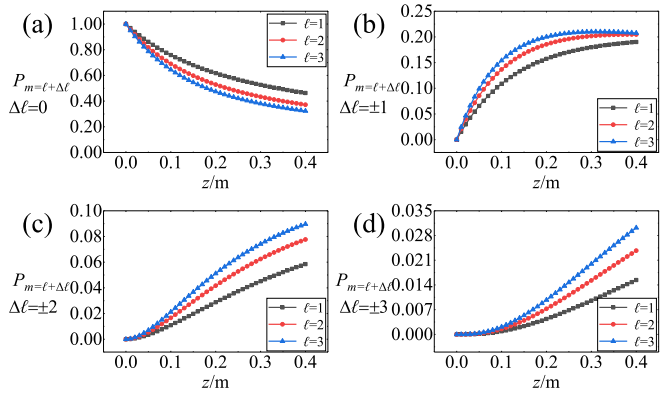

Fig. 2. Detection probability and crosstalk of OAM modes of LG beams with different topological charges (a) $\Delta\ell = 0$, (b–d) $\Delta\ell = \pm 1$, $\Delta\ell = \pm 2$ and $\Delta\ell = \pm 3$, respectively.

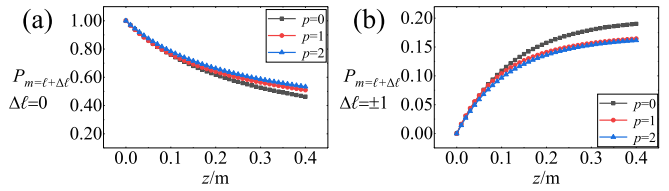

Fig. 3. Detection probability and crosstalk of OAM modes of LG beams with different radial indices (a) $\Delta\ell = 0$, (b) $\Delta\ell = \pm 1$.

the crosstalk is increased as ξ_y decrease. While for Figs. 1(d)–(f), if we fixed $\xi_y = 1$, the crosstalk is decreased as ξ_x increase. When $\xi_x/\xi_y = 1$, the mode crosstalk is the strongest, and the center detection probability $P_{m=1}$ has dropped to 0.22 (Fig. 1(c)). This means that the detection probability of $\ell = 1(\Delta\ell = 0)$ decreases and more energy spread into other adjacent modes ($|\Delta\ell|>0$). The increase of crosstalk can be explained by the phase scrambling by anisotropic plasma turbulence. Regardless of whether ξ_x or ξ_y increases, $T(z)$ in (13) decreases, the turbulence intensity decreases, and the influence on the OAM propagation characteristics will also decrease. In addition, it can be found from (13) that the anisotropy parameter $({\xi_x}^2 + {\xi_y}^2)/{\xi_x}^3{\xi_y}^3$ is symmetrically distributed for the values of ξ_x and ξ_y, which also explains why the Fig. 1(a) and (f), Fig. 1(b) and (d) has the same distribution. With the increase of ξ_x, corresponding to the increase of the vortex eddies perpendicular to the propagation direction of the turbulence, the influence of front and back scattering decreases, thus the OAM crosstalk of LG beam decreases.

Fig. 2(a) shows the variation trend of the detection probability $P_{m=\ell}(\Delta\ell = 0)$ with the propagation length of LG beams with different topological charges. Figs. 2(b), (c), (d) show the crosstalk of adjacent modes $P_{m=\ell+\Delta\ell}(\Delta\ell = \pm 1, \pm 2, \pm 3)$ with the propagation length under different initial topological charges. Except for the $\xi_x/\xi_y = 1$, the other calculation parameters are the same as in Fig. 1. Firstly, it should be noted that regardless of the initial launched topological charge, $P_{m=\ell}$ decreases with the increase of the propagation length, and the corresponding crosstalk increases. However, under a fixed ξ_x/ξ_y, the beam with a larger topological charge ℓ has more obvious crosstalk than a beam with a smaller ℓ. This characteristic is similar to the propagation in atmospheric turbulence. Since the higher-order vortex mode has a larger propagation radius and is exposed to a larger turbulent cross-section, and the phase of the higher-order vortex mode changes faster, it is more likely to crosstalk. In addition, [57] explains this phenomenon with restriction theory, when the OAM quantum number increases, the output power of the incident beam is far away from the axis, which will cause more serious dispersion.

Next, we consider the influence of different radial index p on the spiral spectrum distribution of LG beam propagating in plasma turbulence. It is well known that the different radial index p reflects the number of circular edge dislocations in the phase of LG beam, and appears as dark rings in intensity. When the topological charge ℓ is the same but the radial index p is different, the spot size increases with the increase of p, and the central dark core also decreases.

Fig. 3 shows the variation trend of the detection probability and crosstalk of LG beams with different radial indices p with the propagation length. The calculation parameters are: $\ell = 1$, $\lambda = 1550$ nm, $w_0 = 2$ cm, $\xi_x/\xi_y = 1$, $L_0 = 0.1$ m, $l_0 = 5 \times 10^{-6}$ m, $\langle n_1^2 \rangle = 0.73 \times 10^{-20}$, $R = 3$ cm. It can be found from Fig. 3 that with the increase of the radial index p, the detection probability is higher and the crosstalk is lower at the same propagation length. This is because when p increases, the radius of the dark core in the center of the LG beam decreases, and the ability to resist turbulence is stronger. This means that when the problem of power loss is not considered, a reasonable increase of the radial index p can increase the detection probability of the signal OAM mode and improve the stability of the communication link.

As shown in Fig. 4, the variation of detection probability $P_{m=\ell}$ with the variance and wavelength of turbulence refractive index fluctuation is presented. The calculation parameters are: $\ell = 1$, $w_0 = 2$ cm, $L_0 = 0.1$ m, $l_0 = 5 \times 10^{-6}$ m, $\xi_x/\xi_y = 1$, $R = 3$ cm, $z = 0.4$ m. The variance of refractive index fluctuation

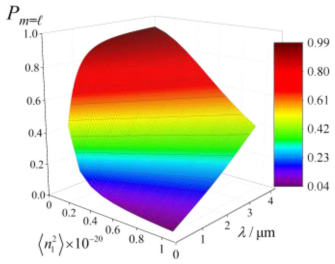

Fig. 4. The dependence of detection probability of OAM mode $P_{m=\ell}$ on the wavelength and the turbulence refractive index fluctuation variance.

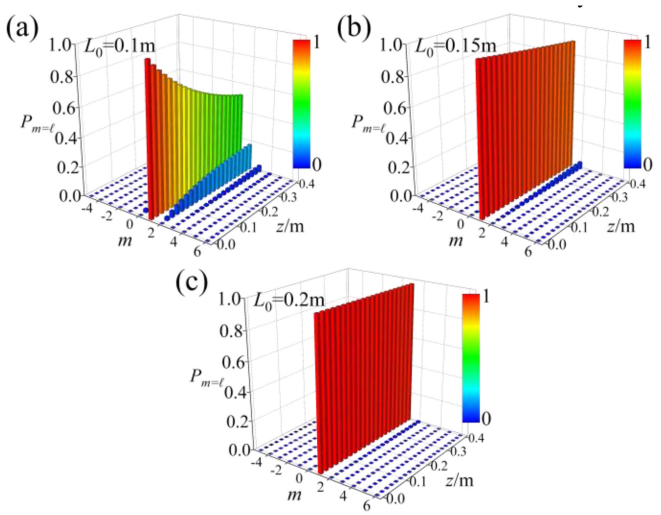

Fig. 5. Detection probability $P_{m=\ell}$ of OAM modes of LG beams with different outer scales (a) $L_0 = 0.1$ m; (b) $L_0 = 0.15$ m and (c) $L_0 = 0.2$ m, respectively.

reflects the physical quantity of turbulence intensity. As the variance of refractive index fluctuation increases, the scattering ability of the turbulent medium increases. Therefore, the detection probability decreases as the variance of refractive index fluctuation increases. In addition, the increase in wavelength will also increase the detection probability. As expected, the long-wavelength beam is less affected by the plasma turbulence and is more suitable for OAM-based communication system.

Fig. 5 displays the dependence of detection probability $P_{m=\ell}$ on the outer scales L_0. The outer scales are 0.1 m, 0.15 m and 0.2 m, and the corresponding inner scales are calculated by (2). The other calculation parameters are: $\ell = 1$, $p = 0$, $\lambda = 1550$ nm, $w_0 = 2$ cm, $\langle n_1^2 \rangle = 0.73 \times 10^{-20}$, $\xi_x/\xi_y = 1$, $R = 3$ cm, $z = 0.4$m. It is well known that compared with the outer scale, the inner scale has a more obvious influence on the beam propagation. This is because the main effect for the outer scale on the beam is to cause random drift of the beam position (beam wander), while the inner scale mainly causes intensity fluctuations (scintillation). As the outer scale increases, according to (2), the inner scale also increases, and the detection probability increases sharply. The drift effect will cause the beam to miss the detector, but the vortex phase can be maintained during the propagation process.

In order to illustrate the influence of the beam width w_0 of the LG beam and the receiving aperture R of the detector on

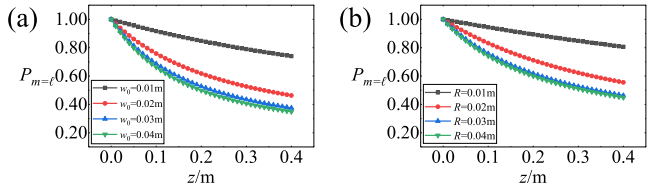

Fig. 6. Detection probability $P_{m=\ell}$ of OAM modes of LG beams (a) with different beam widths and (b) with different receiving aperture.

the detection probability of the plasma turbulence, we display Fig. 6. The calculation parameters are: $\ell = 1, p = 0, \lambda = 1550$ nm, $\langle n_1^2 \rangle = 0.73 \times 10^{-20}$, $l_0 = 5 \times 10^{-6}$ m, $L_0 = 0.1$ m, $\xi_x/\xi_y = 1$. According to Fig. 6(a), as the beam width increases, the detection probability decreases. This is because a larger beam width will be more affected by turbulence, and its OAM link stability will become worse. Therefore, choosing a smaller beam width will increase the detection probability and reduce crosstalk. From Fig. 6(b), as the aperture R increases (the numerator of (15)), the total of the signal carried initially launched OAM modes actually rises. Meanwhile, the denominator of (15) is constructed with primitive transmitting OAM modes and crosstalk among all OAM channels. As the receiving aperture radius R increases, the ratio of the detected OAM signal probability to crosstalk decreases due to the decays with oscillations of LG beams along the radial direction. Thus, the denominator of (15) increases more quickly than the numerator. As a consequence, a larger receiving aperture diameter R leads to a lower detection probability.

V. Quantification of Plasma Turbulence Effect and Comparison With Atmospheric Turbulence Based on Restriction Theory

Ref. [57] shows that the OAM mode weights can only vary in a limited range based on the restriction-characterized function. In addition, they analyze the relationship between the radial distribution of the output beam power and the OAM mode weights in the output OAM spectrum. In this section, we quantify the plasma turbulence based on the proposed restriction characterized function, and finally compared with the atmospheric turbulence.

For each $\Delta\ell$, a restriction-characterized function $\Omega_{\Delta\ell}(r)$ could be given as [57]

$$\Omega_{\Delta\ell}(r) = \frac{D_{\Delta\ell}(r)}{\sum_{\Delta\ell=-\infty}^{\infty} D_{\Delta\ell}(r)}, \tag{18}$$

where

$$D_{\Delta\ell}(r) = \frac{1}{4\pi^2} \int_0^{2\pi} \int_0^{2\pi} \langle \exp[\psi(r, \varphi_1, z) + \psi^*(r, \varphi_2, z)] \rangle \times \exp[-i\Delta\ell(\varphi_1 - \varphi_2)] \, d\varphi_1 d\varphi_2 \tag{19}$$

where $D_{\Delta\ell}(r)$ denotes the influence of the medium on the radial distribution of the incident beam power on the OAM mode with $\Delta\ell$. The denominator $\sum_{\Delta\ell=-\infty}^{\infty} D_{\Delta\ell}(r)$ in (18) reflects the impact of media on the power radial distribution of input beam and should not be zero. In addition, $\Omega_{\Delta\ell}(r)$ requires r to

be restricted to the region M where $\sum_{\Delta\ell=-\infty}^{\infty} D_{\Delta\ell}(r) \neq 0$. In (17), it is evident that the P_m can also be written as an inner product in the region M that

$$P_m = \int_M \Psi(r,z)\,\Omega_{\Delta\ell}(r)dr, \tag{20}$$

where

$$\Psi(r,z) = \frac{|S|^2 \sum_{\Delta\ell=-\infty}^{\infty} D_{\Delta\ell}(r)\,r}{\int_M |S|^2 \sum_{\Delta\ell=-\infty}^{\infty} D_{\Delta\ell}(r)\,rdr}. \tag{21}$$

Eq. (20) indicates that the P_m only depends on two parts: $\Psi(r, z)$ (the radial distribution of normalized output beam power) and $\Omega_{\Delta\ell}(r)$ (the restriction-characterized function). The second part $\Omega_{\Delta\ell}(r)$ is fully determined by the properties of media with each $\Delta\ell$. Essentially, we only consider the impacts of the second part $\Omega_{\Delta\ell}(r)$ on output OAM spectrum in the following discussion, that is, the plasma turbulence effects.

If the OAM mode weight P_m satisfy

$$\inf\{\Omega_{\Delta\ell}(r) | r \in M\} \leq P_m \leq \sup\{\Omega_{\Delta\ell}(r) | r \in M\}. \tag{22}$$

where $\sup\{\Omega_{\Delta\ell}(r)\}$ and $\inf\{\Omega_{\Delta\ell}(r)\}$ are the upper and lower bounds respectively. If the transmission function (plasma turbulence or atmospheric turbulence) is explicitly determined, the upper or lower bounds for each $\Delta\ell$ will be fixed.

To obtain $\Omega_{\Delta\ell}(r)$ of the atmospheric turbulence, theoretical derivation will begin with the well-known non-Kolmogorov spectral model. Considering the ensemble average and using the quadratic approximation, then

$$\begin{aligned}&\langle \exp[\psi(r,\varphi_1,z) + \psi^*(r,\varphi_2,z)]\rangle_{AT} \\ &\quad = \exp\left[-2r^2 T_{AT}(z) + 2r^2 T_{AT}(z)\cos(\varphi_1-\varphi_2)\right]\end{aligned} \tag{23}$$

where $T_{AT}(z) = 1/\rho_0^2$ and ρ_0 is the spatial coherence radius for a plane or spherical wave in non-Kolmogorov turbulence [49]. Then

$$\Omega_{\Delta\ell}(r)_{AT} = \exp\left[-2r^2 T_{AT}(z)\right] I_{\Delta\ell}\left[2r^2 T_{AT}(z)\right] \tag{24}$$

while for plasma turbulence

$$\Omega_{\Delta\ell}(r)_{PT} = \exp\left[-2r^2 T_{PT}(z)\right] I_{\Delta\ell}\left[2r^2 T_{PT}(z)\right] \tag{25}$$

where the subscript AT or PT indicate atmospheric turbulence and plasma turbulence, respectively. By calculating the $\inf\{\Omega_{\Delta\ell}(r)\}$ and $\sup\{\Omega_{\Delta\ell}(r)\}$ in (24) and (25), the upper or lower bounds of OAM mode weights for each $\Delta\ell$ are irrelevant to the intensity of phase fluctuation $T(z)$. However, due to the difference in turbulence models, the radial dimension r is quite different when $\Omega_{\Delta\ell}(r)$ reach its upper bound. We have added this distinction in this section and pointed out the difference between plasma turbulence effects and atmospheric turbulence effects.

We give the varying range of output OAM spectrum with different $\Delta\ell$ in Table I, in which the upper bounds are calculated by (24) and (25). For all $\Delta\ell$, its lower bounds is 0, as $\inf\{\Omega_{\Delta\ell}(r)|r\in M\} = \lim_{r\to+\infty}\Omega_{\Delta\ell}(r) = 0$. These lower or upper bounds are intrinsic and unique because they are independent of any characteristics of input LG beam and even the intensity of turbulence. The spatial coherence radius of atmospheric turbulence $\rho_0 = 0.9$m. It can be observed from the second and third rows of Table I that the upper bounds of the atmospheric and plasma turbulence are the same constrained by the Bessel function I_n. The upper bound drops rapidly as $|\Delta\ell|$ increases. However, it can be seen from the third and fourth rows in Table I that in atmospheric and plasma turbulence, the values of r when $\Omega_{\Delta\ell}(r)$ reach these upper bounds are very different. For the same $|\Delta\ell|$, the value of r at the upper bound of atmospheric turbulence is greater than that of plasma turbulence 12 times. The effect of plasma turbulence has a greater impact on OAM spectrum spread. Physically, the radial dimension r will increase in any types of turbulence. The beam spreading effect also exists even in free space transmission although it's changed little. We know that both the scintillation and spreading effects of beam are related to the fluctuations in intensity. When $\Omega_{\Delta\ell}(r)$ reaches this upper bound, the value of r is significantly advanced, this means that the increase in the radial dimension r (or intensity fluctuations) of the beam caused by plasma turbulence is more obvious.

TABLE I
THE UPPER BOUNDS OF OUTPUT OAM MODE WEIGHTS FOR $|\Delta\ell| = 0$ TO 5 (DEFINED BY EQ. (24) AND EQ. (25)) AND THE VALUE OF r WHEN $\Omega_{\Delta\ell}(r)$ REACHES UPPER BOUND, WHERE AT: ATMOSPHERIC TURBULENCE AND PT: PLASMA TURBULENCE

$\lvert\Delta\ell\rvert$	0	1	2	3	4	5
upper bound (AT)	1.000	0.219	0.118	0.080	0.060	0.048
upper bound (PT)	1.000	0.219	0.118	0.080	0.060	0.048
r when $\Omega_{\Delta\ell}(r)$ reaches upper bound (AT)/m	0.000	0.804	1.383	2.000	2.630	3.270
r when $\Omega_{\Delta\ell}(r)$ reaches upper bound (PT)/m	0.000	0.066	0.114	0.165	0.217	0.270

We chose another set of atmospheric turbulence parameter to reflect the influence of the two turbulences on the OAM spectrum. The spatial coherence radius of atmospheric turbulence $\rho_0 = 0.14$m, which indicates moderate-to-strong turbulence strength. The comparison result is shown in Fig. 7.

Fig. 7 shows the distribution of $\Omega_{\Delta\ell}(r)$ with r under different $|\Delta\ell|$ (a, b, c) and the spectrum distribution of LG beam propagating in atmospheric turbulence and plasma turbulence (d). It can be observed from Fig. 7(a) that with the increase of r, the downward trend of $\Omega_{\Delta\ell}(r)$ in plasma turbulence is steeper than that in atmospheric turbulence. While in Figs. 7(b) and (c), the values of r in plasma turbulence when $\Omega_{\Delta\ell}(r)$ reach its upper bound is always smaller than that in atmospheric turbulence. Even in the strong turbulence region of atmospheric turbulence, the strength of plasma turbulence is twice as strong as atmospheric turbulence. The plasma turbulence effect is more obvious in Fig. 7(d), which compares the spiral spectrum of the LG beam propagating in atmospheric turbulence and plasma turbulence. It can be seen from Fig. 7(d) that the spiral spectrum

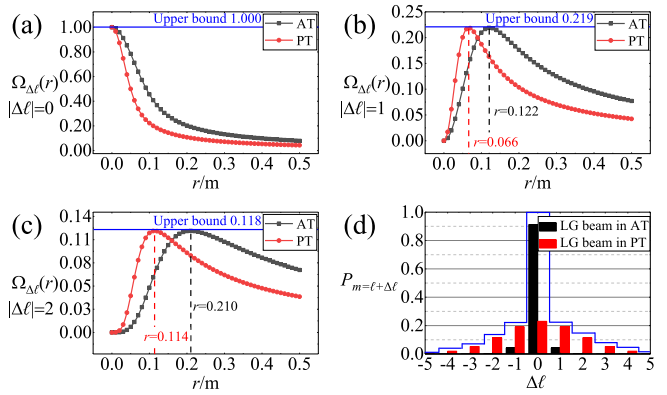

Fig. 7. The distribution of $\Omega_{\Delta\ell}(r)$ with r under different $|\Delta\ell|$ (a, b, c) and the spectrum distribution of LG beam propagating in atmospheric turbulence and plasma turbulence (d), where AT: atmospheric turbulence and PT: plasma turbulence.

of the LG beam propagating in plasma turbulence is more spread than that of atmospheric turbulence, and the signal OAM mode is significantly lower. At this time, the modes crosstalk has almost reached its upper bound (see the solid blue line in Fig. 7(d)), indicating that the LG beam is more severely affected by plasma turbulence.

VI. Comparison on Optimization of Detection Probability Using Circular Aperture Method and Focusing Mirror Method

We optimize the OAM detection probability and crosstalk based on the method reported in [58] and [59]. These two optimization methods: circular aperture method (CAM) and focusing mirror method (FMM) are shown in Fig. 8. It is worth noting that there are many optimization schemes reported for OAM detection probability and crosstalk. In addition to the choice of beams and source parameters or adaptive optics scheme, the purpose of CAM is to optimize on the receiving plane, while the FMM is to optimize on the initial plane. The goal of this paper is to propose the selection criteria for these two schemes in anisotropic plasma turbulent media, and give which method should be selected under what conditions is helpful to resist the turbulence effect and maintain the signal OAM transmission efficiency.

A. Circular Aperture Method (CAM)

For the CAM, as shown in Fig. 8(a), a circular aperture can be used at the receiving plane to filter the crosstalk from the adjacent OAM modes. Summing the complex Gaussian functions, the function of a circular aperture could be obtained as [55]

$$H(r) = \sum_{t=1}^{10} A_t \exp\left(-\frac{B_t}{a^2} r^2\right) \tag{26}$$

where a is the radius of a circle aperture, A_t and B_t are the expansion and Gaussian coefficients, respectively, from the [60],

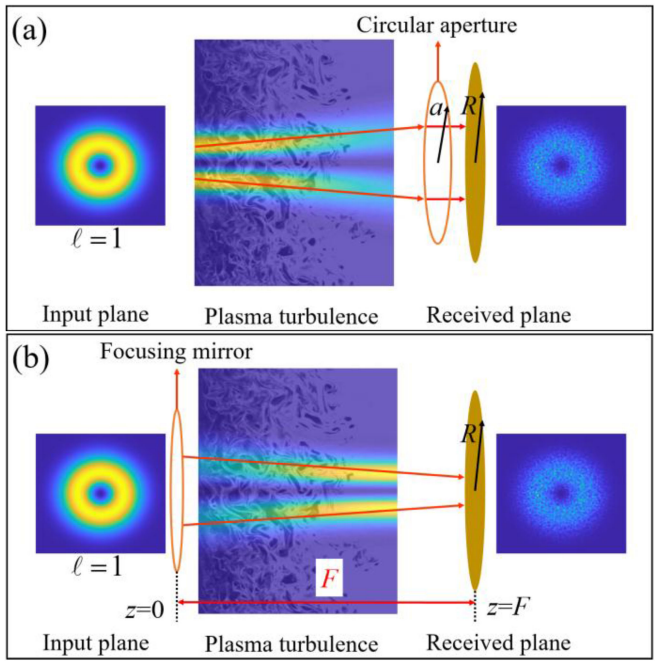

Fig. 8. Schematic diagram of using (a) CAM and (b) FMM to optimize the OAM mode detection probability.

[61]. At this time, the coefficient C_m in (16) becomes

$$C_m = \sum_{t=1}^{10}\sum_{t'=1}^{10} A_t A_{t'}^* \int \left\langle |\beta_m(r,z)|^2 \right\rangle \times \exp\left(-\frac{B_t + B_{t'}^*}{a^2} r^2\right) r dr \tag{27}$$

B. Focusing Mirror Method (FMM)

For the FMM, as shown in Fig. 8(b), a light beam with vortex phase passes through a focusing mirror and then propagates in plasma turbulence. We can add an exponential term to the initial plane to represent the effect of the focusing mirror as [62], [63]

$$E(r,\varphi,0) = LG_p^{(\ell)}(r,\varphi,0) \exp\left(-\frac{iC_0}{2w_0^2} r^2\right) \tag{28}$$

where $C_0 = kw_0{}^2/F$ is the initial beam prefocusing parameter and F is the focal distance or the distance from the initial plane to the receiver plane.

C. Selection Criterion of CAM and FMM in Plasma Turbulence

Fig. 9 displays the comparison of OAM modes detection probability between the optimization or not by using the CAM and the FMM. The calculation parameters are as follows: $\ell = 1$, $p = 0$, $\lambda = 1550$ nm, $w_0 = 2$ cm, $L_0 = 0.1$ m, $l_0 = 5\times10^{-6}$m, $\xi_x = \xi_y = 1$, $\langle n_1^2 \rangle = 0.73 \times 10^{-20}$, $R = 3$ cm, $z = 0.4$ m, $a = 25$ mm, $F = 0.4$ m. It can be observed from Fig. 9 that the OAM modes detection probability is improved after using the CAM and FMM. With the CAM, compared with no

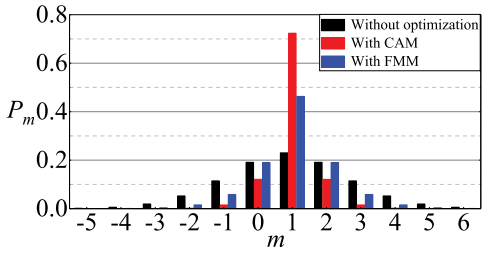

Fig. 9. Comparison of the detection probability after optimization using the CAM and FMM and without optimization.

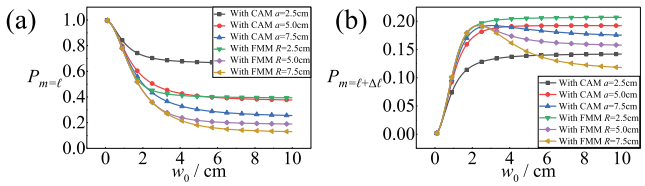

Fig. 10. The variation trend of the detection probability (a) and crosstalk (b, $\Delta\ell = \pm 1$) of the CAM and FMM with the beam width under different receiving apertures.

optimization, the center mode detection probability $P_{m\,=\,1}$ has exceeded 0.7, which is increased by 0.5 compared with the case without optimization. While with the FMM, its $P_{m\,=\,1}$ reaches 0.46, which is increased by 0.2 compared with the case without optimization. This means that with a CAM at the receiving plane or adding a FMM at the initial plane can significantly increase the detection probability, reduce OAM modes crosstalk and improve the communication quality of the beam in plasma turbulence. In order to understand the influence of the two methods on the OAM modes, we will give a comparison.

Fig. 10 displays the variation trend of the detection probability and crosstalk of the two methods with the beam width under different receiving apertures. It can be seen from Fig. 10(a) that under different receiving apertures, as the beam width increases, the detection probability shows a decreasing trend, and it stabilizes after decreasing to a certain extent. Regardless of the CAM or the FMM, the smaller the aperture, the higher the detection probability. Under the same receiving aperture, the detection probability optimized by the CAM is always higher than that by the FMM. It can be observed from Fig. 10(b) that when the receiving aperture $a = R = 2.5$ cm, the crosstalk of using the FMM is greater than the crosstalk of using the CAM. In the case of large aperture, when $a = R = 5.0$ cm or 7.5 cm, there is a critical beam width w_0 and aperture a or R, so that when the beam width is greater than this critical value, the crosstalk of using the FMM is lower than that of using the CAM. We found the distribution of this critical value and display Fig. 11.

Fig. 11(a) displays the dependence of crosstalk probability ($\Delta\ell = \pm 1$) on the beam width w_0 and the receiving aperture a or R under the optimization of the CAM and FMM. It can be observed that under the small beam width or small receiving aperture, the crosstalk of using the FMM is always greater than that of using the CAM. The situation is different when the beam width and receiving aperture increase. We marked the

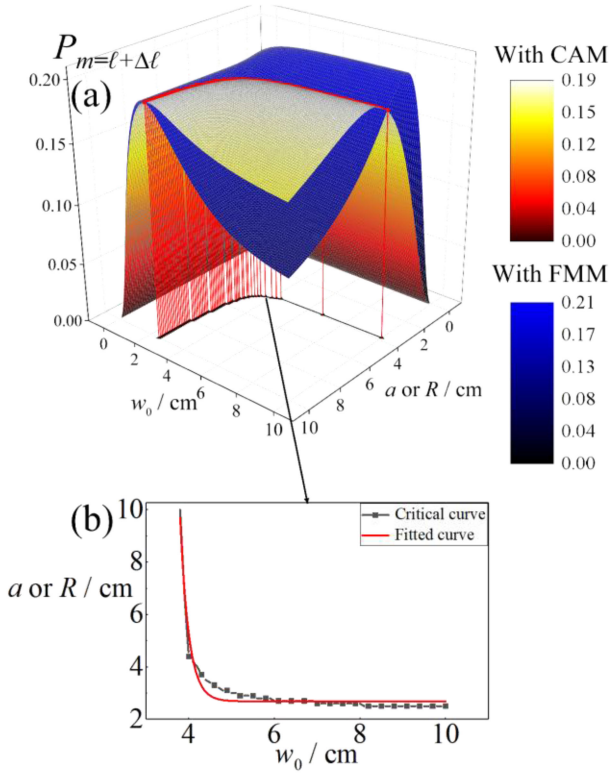

Fig. 11. The dependence of crosstalk probability $P_{m\,=\,\ell+\Delta\ell}(\Delta\ell = \pm 1)$ optimized by the CAM and the FMM on the beam width w_0 and the receiving aperture a or R (a) and 2D critical value curve and fitting curve (b).

intersection of two surfaces with a red line in the figure. On the front side of this line of intersection (e.g., $w_0 \geq$2.5 cm, a or $R \geq$3.8 cm), the crosstalk optimized by the FMM is smaller than that by the CAM. Therefore, it is necessary to find out the relationship between this critical beam width and aperture to achieve the choice of different methods. Based on this, we drew and fitted the relationship between this critical value in Fig. 11(b). Fig. 11(b) displays the 2D distribution of the critical value of the beam width w_0 and the aperture a (i.e., the intersection of the curved surface in Fig. 11(a)). We show the curve fitted with an exponential function (red line), and the fitted curve is given in the following form

$$a = y_0 + A_0 \exp\left(R_0 w_0\right) \tag{29}$$

where

$$y_0 = 0.02685 \pm 3.2858 \times 10^{-4} \tag{30}$$

$$A_0 = 1.0583 \times 10^7 \pm 1.19978 \times 10^7 \tag{31}$$

$$R_0 = -495.57463 \pm 29.42006 \tag{32}$$

When the value of the beam width w_0 (or aperture a) is fixed, there is a critical aperture a (or beam width w_0). When the value of a (or w_0) is greater than this critical value, the crosstalk optimized using the FMM will be less than that using the CAM. Therefore, when considering the choice of optimization method, in addition to considering the influence of source parameters, one can determine the appropriate combination of beam width and

aperture to choose different methods. When the beam width $w_0 \geq 4$ cm and the aperture a or $R \geq 3$ cm, the FMM has a greater ability to reduce crosstalk than the CAM.

We also calculated other parameters such as wavelength from 633nm to 1550nm and topological charge from 1 to 5, found that this critical value is not sensitive to wavelength and topological charge. Therefore, calculations under similar circumstances have similar conclusions. The selection method of CAM and FMM in this paper can also be extended to atmospheric turbulence. The results may be useful in the field of OAM based communication system in plasma turbulence, and we provide a guideline for the selection of these two parameters.

VII. Conclusion

In this paper, we have derived a theoretical expression for calculating the spiral spectrum of LG beam propagation through anisotropic plasma turbulence. On the basis of the derived model, the specific influence of source parameters (such as topological charge, radial index and wavelength, etc.) and turbulence parameters (such as the anisotropy coefficient, refractive index fluctuation variance, inner and outer scales) on the OAM detection probability and crosstalk have been investigated. Based on these analyses, reducing the topological charge, increasing the radial index, utilizing a long wavelength, reducing the beam width or receiving aperture are applicable to improve the detection probability. We quantified the effect of plasma turbulence and pointed out the difference between the plasma turbulence and atmospheric turbulence on OAM spiral spectrum. In addition, the effects of the circular aperture method and focusing mirror method on detection probability and crosstalk are also presented. Through comparing these two methods, it is found that the ability to reduce the crosstalk of the two methods is related to the combination of beam width and receiving aperture. We give a method and criteria for choosing these two optimization methods. When the beam width ≥ 4 cm and the aperture ≥ 3 cm, the focusing mirror method has a greater ability to reduce crosstalk than the circular aperture method. Our results provide a guideline for the selection of these two parameters and methods. The results may be useful for the establishment of OAM based optical communication system in anisotropic plasma turbulence.

References

[1] J. P. Rybak and R. J. Churchill, "Progress in reentry communications," *IEEE Trans. Aerosp. Electron. Syst.*, vol. AES-7, no. 5, pp. 879–894, Sep. 1971.

[2] R. Hartunian, G. E. Stewart, S. D. Fergason, T. J. Curtis, and R. W. Seibold, "Causes and mitigation of radio frequency (RF) blackout during reentry of reusable launch vehicles," Aerospace Corp., EI Segundo, CA, USA, Tech. Rep. ATR-2007(5309)-1, Jan. 2007.

[3] R. P. Starkey, "Hypersonic vehicle telemetry blackout analysis," *J. Spacecr. Rockets*, vol. 52, no. 2, pp. 426–438, 2015.

[4] K. Yuan, L. Shen, M. Yao, X. Deng, Z. Chen, and L. Hong, "Studies on the transmission of sub-THz waves in magnetized inhomogeneous plasma sheath," *Phys. Plasmas*, vol. 25, no. 1, 2018, Art. no. 013302.

[5] R. Tang, M. Mao, K. Yuan, Y. Wang, and X. Deng, "A terahertz signal propagation model in hypersonic plasma sheath with different flight speed," *Phys. Plasmas*, vol. 26, no. 4, 2019, Art. no. 043509.

[6] W. Chen, L. Yang, Z. Huang, and L. Guo, "Propagation characteristics of THz waves in space-time inhomogeneous and fully ionized dusty plasma sheath," *J. Quant. Spectrosc. Radiat. Transfer*, vol. 232, pp. 66–74, 2019.

[7] H. Li, W. Ding, J. Liu, L. Bai, and Z. Wu, "OAM crosstalk of multiple coaxial THz vortex beams propagating through an inhomogeneous unmagnetized plasma slab," *Phys. Plasmas*, vol. 26, no. 12, 2019, Art. no. 123507.

[8] Q. Zang *et al.*, "Phase characteristic and information transmission of laser signals through plasma in shock tube," *Phys. Plasmas*, vol. 26, no. 2, 2019, Art. no. 022107.

[9] Q. Zang *et al.*, "Laboratory simulation of laser propagation through plasma sheaths containing ablation particles of ZrB_2-SiC-C during hypersonic flight," *Opt. Lett*, vol. 42, no. 4, pp. 687–690, 2017.

[10] N. G. Bykova *et al.*, "Experimental demonstration of the feasibility of laser communication with reentry spacecraft at 1.55 um," *Appl. Opt*, vol. 56, no. 10, pp. 2597–2603, 2017.

[11] T. Wang, Y. Zhao, D. Xu, and Q. Yang, "Numerical study of evaluating the optical quality of supersonic flow fields," *Appl. Opt.*, vol. 46, no. 23, pp. 5545–5551, 2007.

[12] Q. Gao, Z. Jiang, S. Yi, and Y. Zhao, "Optical path difference of the supersonic mixing layer," *Appl. Opt.*, vol. 49, no. 19, pp. 3786–3792, 2010.

[13] H. Ding, S. Yi, X. Zhao, J. Yi, and L. He, "Research on aero-optical prediction of supersonic turbulent boundary layer based on aero-optical linking equation," *Opt. Exp.*, vol. 26, no. 24, pp. 31317–31332, 2018.

[14] G. Guo, H. Liu, and B. Zhang, "Development of a temporal evolution model for aero-optical effects caused by vortices in the supersonic mixing layer," *Appl. Opt.*, vol. 55, no. 10, pp. 2708–2717, 2016.

[15] G. Guo, H. Liu, and B. Zhang, "Aero-optical effects of an optical seeker with a supersonic jet for hypersonic vehicles in near space," *Appl. Opt.*, vol. 55, no. 17, pp. 4741–4751, 2016.

[16] V. A. Banakh, A. A. Sukharev, and A. V. Falits, "Optical beam distortions induced by a shock wave," *Appl. Opt.*, vol. 54, no. 8, pp. 2023–2031, 2015.

[17] A. A. Sukharev, G. G. Matvienko, and O. A. Romanovskii, "Distortion of a laser beam propagating through a shock wave formed by a supersonic flow around an aerodynamic body in a homogeneous medium and a turbulent atmosphere," in *Proc. 25th Int. Symp. Atmospheric Ocean Opt.: Atmospheric Phys.*, 2019, Art. no. 1120819.

[18] Y. Min, L. Xiaoping, X. Kai, L. Yanming, and L. Donglin, "A large volume uniform plasma generator for the experiments of electromagnetic wave propagation in plasma," *Phys. Plasmas*, vol. 20, no. 1, 2013, Art. no. 012101.

[19] M. M. Hatami, "Sheath structure in plasmas with nonextensively distributed electrons and thermal ions," *Phys. Plasmas*, vol. 22, no. 2, 2015, Art. no. 023506.

[20] A. Mousavi, A. Esfandiari-Kalejahi, and M. Akbari-Moghanjoughi, "Optical properties of nonextensive inhomogeneous plasma sheath," *Phys. Plasmas*, vol. 23, no. 7, 2016, Art. no. 073511.

[21] A. Mousavi, A. Esfandiari-Kalejahi, and M. Akbari-Moghanjoughi, "Nonextensivity effect on radio-wave transmission in plasma sheath," *Phys. Plasmas*, vol. 23, no. 4, 2016, Art. no. 043516.

[22] L. Dan, L. X. Guo, and J. T. Li, "Propagation characteristics of electromagnetic waves in dusty plasma with full ionization," *Phys. Plasmas*, vol. 25, no. 1, 2018, Art. no. 013707.

[23] J. Feng, C. Shen, and Q. Wang, "Three-dimensional evolution of large-scale vortices in supersonic flow," *Appl. Phys. Lett.*, vol. 107, no. 25, 2015, Art. no. 254101.

[24] H. Ding, S. Yi, Y. Zhu, and L. He, "Experimental investigation on aero-optics of supersonic turbulent boundary layers," *Appl. Opt.*, vol. 56, no. 27, pp. 7604–7610, 2017.

[25] J. Li, S. Yang, and L. Guo, "Propagation characteristics of Gaussian beams in plasma sheath turbulence," *IET Microw. Antennas Propag.*, vol. 11, no. 2, pp. 280–286, 2017.

[26] J. Li, S. Yang, L. Guo, M. Cheng, and T. Gong, "Bit error rate performance of free-space optical link under effect of plasma sheath turbulence," *Opt. Commun.*, vol. 396, pp. 1–7, 2017.

[27] C. J. Lyu and Y. P. Han, "Analysis of propagation characteristics of Gaussian beams in turbulent plasma sheaths," *Acta Phys. Sin.*, vol. 68, no. 9, 2019, Art. no. 094201.

[28] Y. Zhao, S. Yi, L. Tian, L. He, and Z. Cheng, "The fractal measurement of experimental images of supersonic turbulent mixing layer," *Sci. China, Ser. G: Phys., Mech. Astron.*, vol. 51, no. 8, pp. 1134–1143, 2008.

[29] J. Li, S. Yang, L. Guo, and M. Cheng, "Anisotropic power spectrum of refractive-index fluctuation in hypersonic turbulence," *Appl. Opt.*, vol. 55, no. 32, pp. 9137–9144, 2016.

[30] X. Huang, S. Nan, W. Tan, Y. Bai, and X. Fu, "Statistical properties of gaussian Schell-model beams propagating through anisotropic hypersonic turbulence," *OSA Continuum.*, vol. 2, no. 12, pp. 3584–3597, 2019.

[31] L. Allen, M. W. Beijersbergen, R. J. Spreeuw, and J. P. Woerdman, "Orbital angular momentum of light and the transformation of Laguerre-Gaussian laser modes," *Phys. Rev.*,vol. 45, no. 11, pp. 8185–8189, 1992.

[32] L. Gong *et al.*, "Optical orbital-angular-momentum-multiplexed data transmission under high scattering," *Light. Sci. Appl.*, vol. 8, pp. 27–38, 2019.

[33] Q. Tian, L. Zhu, Y. Wang, Q. Zhang, B. Liu, and X. Xin, "The propagation properties of a longitudinal orbital angular momentum multiplexing system in atmospheric turbulence," *IEEE Photon. J.*, vol. 10, no. 1, Feb. 2018, Art. no. 7900416.

[34] J. Zhou, J. Wu, J. Zong, and Q. Hu, "Optimal mode set selection for free space optical communications in the presence of atmosphere turbulence," *J. Lightw. Technol.*, vol. 36, no. 11, pp. 2222–2229, Jun. 2018.

[35] M. A. Cox, L. Maqondo, R. Kara, G. Milione, L. Cheng, and A. Forbes, "The resilience of hermite– and Laguerre–Gaussian modes in turbulence," *J. Lightw. Technol.*, vol. 37, no. 16, pp. 3911–3917, Aug. 2019.

[36] Y. Weng, Y. Guo, O. Alkhazragi, T. K. Ng, J. H. Guo, and B. S. Ooi, "Impact of turbulent-flow-induced scintillation on deep-ocean wireless optical communication," *J. Lightw. Technol.*, vol. 37, no. 19, pp. 5083–5090, Oct. 2019.

[37] H. Song *et al.*, "Experimental mitigation of atmospheric turbulence effect using pre-signal combining for Uni- and Bi-directional free-space optical links with two 100-Gbit/s OAM-Multiplexed channels," *J. Lightw. Technol.*, vol. 38, no. 1, pp. 82–89, Jan. 2020.

[38] B. Yan *et al.*, "Orbital angular momentum (OAM) carried by asymmetric vortex beams for wireless communications: Theory, experiment and current challenges," *IEEE J. Sel. Topics Quantum Electron.*, vol. 27, no. 2, Mar./Apr. 2021, Art. no. 7600310.

[39] G. Gbur and R. K. Tyson, "Vortex beam propagation through atmospheric turbulence and topological charge conservation," *J. Opt. Soc. Amer. A*, vol. 25, no. 1, pp. 225–230, 2008.

[40] J. Zeng, X. Liu, C. Zhao, F. Wang, G. Gbur, and Y. Cai, "Spiral spectrum of a Laguerre-Gaussian beam propagating in anisotropic non-Kolmogorov turbulent atmosphere along horizontal path," *Opt. Exp.*, vol. 27, no. 18, pp. 25342–25356, 2019.

[41] M. Cheng, L. Guo, J. Li, X. Yan, R. Sun, and Y. You, "Effects of asymmetry atmospheric eddies on spreading and wander of Bessel–Gaussian beams in anisotropic turbulence," *IEEE Photon. J.*, vol. 10, no. 3, Jun. 2018, Art. no. 6100510.

[42] Y. Li, Y. Zhang, and Y. Zhu, "Lommel-Gaussian pulsed beams carrying orbital angular momentum propagation in asymmetric oceanic turbulence," *IEEE Photon. J.*, vol. 12, no. 1, Feb. 2020, Art. no. 7900915.

[43] P. Gao, L. Bai, Z. Wang, Z. Wu, and L. Guo, "Evolution behavior of mixed higher order optical vortex–edge dislocations propagating through atmospheric turbulence," *IEEE Photon. J.*, vol. 10, no. 3, Jun. 2018, Art. no. 7904510.

[44] J. Li, J. Li, L. Guo, M. Cheng, and L. Xi, "Polarization characteristics of radially polarized partially coherent vortex beam in anisotropic plasma turbulence," *Waves Random Complex Media*, vol. 30, pp. 1–14, 2020.

[45] L. Xu, Y. Xin, Z. Zhou, T. Ren, and B. Han, "Propagation characteristics of orbital angular momentum and its time evolution carried by a Laguerre-Gaussian beam in supersonic turbulent boundary layer," *Opt. Exp.*, vol. 28, no. 3, pp. 4032–4047, 2020.

[46] A. N. Shahrbabaki, M. Bazazzadeh, M. D. Manshadi, and A. Shahriari, "Designing a fuzzy logic controller for the reynolds number in a blowdown supersonic wind tunnel," in *Proc. IEEE Aerosp. Conf.*, 2014, pp. 1–12.

[47] S. C. Lin, "Spectral characterization of dielectric constant fluctuation in hypersonic wake plasmas," *AIAA J.*, vol. 7, no. 10, pp. 1853–1861, 1969.

[48] A. M. Yao and M. J. Padgett, "Orbital angular momentum: Origins, behavior and applications," *Adv. Opt. Photon.*, vol. 3, no. 2, pp. 161–204, 2011.

[49] L. Torner, J. P. Torres, and S. Carrasco, "Digital spiral imaging," *Opt. Exp.*, vol. 13, no. 3, pp. 873–881, 2005.

[50] Y. Li, L. Yu, and Y. Zhang, "Influence of anisotropic turbulence on the orbital angular momentum modes of Hermite-Gaussian vortex beam in the ocean," *Opt. Exp.*, vol. 25, no. 11, pp. 12203–12215, 2017.

[51] L. C. Andrews and R. L. Phillips, *Laser Beam Propagation through Random Media*, Bellingham, WA USA: The International Society for Optical Engineering Press, 2005.

[52] C. Paterson, "Atmospheric turbulence and orbital angular momentum of single photons for optical communication," *Phys. Rev. Lett.*, vol. 94, no. 15, 2005, Art. no. 153901.

[53] H. T. Yura, "Mutual coherence function of a finite cross section optical beam propagating in a turbulent medium," *Appl. Opt.*, vol. 11, no. 6, pp. 1399–1406, 1972.

[54] V. I. Tatarskii, *Wave Propagation in Turbulent Medium*. New York, NY, USA: McGraw-Hill, 1961.

[55] H. I. Sztul and R. R. Alfano, "The poynting vector and angular momentum of airy beams," *Opt. Exp.*, vol. 16, no. 13, pp. 9411–9416, 2008.

[56] Y. D. Liu, C. Gao, M. Gao, and F. Li, "Coherent-mode representation and orbital angular momentum spectrum of partially coherent beam," *Opt. Commun.*, vol. 281, no. 8, pp. 1968–1975, 2008.

[57] T. Zhang, Y. D. Liu, K. Yang, J. Wang, P. Liu, and Y. Yang, "Restriction on orbital angular momentum distribution: A role of media in vortex beams propagation," *Opt. Exp.*, vol. 26 no. 13, pp. 17227–17235, 2018.

[58] Y. Yuan, D. Liu, Z. Zhou, H. Xu, J. Qu, and Y. Cai, "Optimization of the probability of orbital angular momentum for laguerre-gaussian beam in kolmogorov and non-Kolmogorov turbulence," *Opt. Exp.*, vol. 26, no. 17, pp. 21861–21871, 2018.

[59] M. Zhou, Y. Zhou, G. Wu, and Y. Cai, "Reducing the cross-talk among different orbital angular momentum modes in turbulent atmosphere by using a focusing mirror," *Opt. Exp.*, vol. 27, no. 7, pp. 10280–10287, 2019.

[60] J. J. Wen and M. A. Breazeale, "A diffraction beam field expressed as the superposition of gaussian beams," *J Acoust Soc. Amer.*, vol. 83, no. 5, pp. 1752–1756, 1988.

[61] D. Ding and X. Liu, "Approximate description for bessel, bessel–gauss, and gaussian beams with finite aperture," *J. Opt. Soc. Amer. A*, vol. 16, no. 6, pp. 1286–1293, 1999.

[62] Y. Cai and L. Hu, "Propagation of partially coherent twisted anisotropic gaussian Schell-model beams through an apertured astigmatic optical system," *Opt. Lett.*, vol. 31, no. 6, pp. 685–687, 2006.

[63] A. M. Rubenchik, M. P. Fedoruk, and S. K. Turitsyn, "Laser beam self-focusing in the atmosphere," *Phys. Rev. Lett.*, vol. 102, no. 23, 2009, Art. no. 233902.